



5-2016

Prandtl Number Effect on Assisted Convective Heat Transfer through a Solar Collector

Rehen Nasrin
Bangladesh University of Engineering & Technology

Salma Parvin
Bangladesh University of Engineering & Technology

M. A. Alim
Bangladesh University of Engineering & Technology

Follow this and additional works at: <https://digitalcommons.pvamu.edu/aam>



Part of the [Numerical Analysis and Computation Commons](#)

Recommended Citation

Nasrin, Rehen; Parvin, Salma; and Alim, M. A. (2016). Prandtl Number Effect on Assisted Convective Heat Transfer through a Solar Collector, *Applications and Applied Mathematics: An International Journal (AAM)*, Vol. 11, Iss. 3, Article 3.

Available at: <https://digitalcommons.pvamu.edu/aam/vol11/iss3/3>

This Article is brought to you for free and open access by Digital Commons @PVAMU. It has been accepted for inclusion in *Applications and Applied Mathematics: An International Journal (AAM)* by an authorized editor of Digital Commons @PVAMU. For more information, please contact hvkoshy@pvamu.edu.



Available at
<http://pvamu.edu/aam>
Appl. Appl. Math.
ISSN: 1932-9466

Applications and
Applied Mathematics:
An International Journal
(AAM)

Special Issue No. 2 (May 2016), pp. 22 – 36

18th International Mathematics Conference, March 20 – 22, 2014, IUB Campus, Bashundhara
Dhaka, Bangladesh

Prandtl Number Effect on Assisted Convective Heat Transfer through a Solar Collector

Rehena Nasrin^{*}, Salma Parvin and M.A. Alim

Department of Mathematics
Bangladesh University of Engineering & Technology
Dhaka-1000, Bangladesh

*Email: rehena@math.buet.ac.bd

ABSTRACT

Numerical study of the influence of Prandtl number on forced convective heat transfer through a riser pipe of a flat plate solar collector is done. The working fluid is $\text{Al}_2\text{O}_3/\text{water}$ nanofluid. By Finite Element Method the governing partial differential equations are solved. The effect of the Prandtl number on the temperature and velocity field has been depicted. Comprehensive average Nusselt number, average bulk temperature, mean velocity, mid-height temperature inside the pipe, mean output temperature and collector efficiency are presented for the governing parameter mentioned above. Nu increases by 16% with the variation of Pr from 4.6 to 6.6 using nanofluid. Due to rising Pr heat transfer rate increases but collector efficiency devalues.

KEYWORDS: Assisted convection, finite element method, water- Al_2O_3 nanofluid, thermal efficiency

MSC 2010 No.: 65, 76

1. INTRODUCTION

Solar collectors are key elements in many applications, such as building heating systems, solar drying devices, etc. Solar energy has the greatest potential of all the sources of renewable energy especially when other sources in the country have depleted. The fluids with solid-sized nanoparticles suspended in them are called “nanofluids.” The suspended metallic or nonmetallic

nanoparticles change the transport properties and heat transfer characteristics of the base fluid. Nanofluids are expected to exhibit superior heat transfer properties compared with conventional heat transfer fluids. Forced convection occurs when a fluid flow is induced by an external force. In other words, it is a mechanism in which fluid motion is generated by an external source (like a pump, fan or mixer, suction device etc.). Significant amounts of heat energy can be transported very efficiently by this system and it is found very commonly in everyday life, including central heating, air conditioning, steam turbines and in many other machines.

Struckmann (2008) analyzed flat-plate solar collector where efforts had been made to combine a number of the most important factors into a single equation and thus formulate a mathematical model which would describe the thermal performance of the collector in a computationally efficient manner. Zambolin (2011) theoretically and experimentally performed solar thermal collector systems and components. Sandhu (2013) experimentally studied temperature field in flat-plate collector and heat transfer enhancement with the use of insert devices. Various new configurations of the conventional insert devices were tested over a wide range of Reynolds number (200-8000). Chabane et al. (2013) studied thermal performance optimization of a flat plate solar air heater. The received energy and useful energy rates of the solar air heaters were evaluated for various air flow rates were (0.0108, 0.0145, 0.0161, 0.0184 and 0.0203 kg.s⁻¹) are investigated. Optimum values of air mass flow rates were suggested maximizing the performance of the solar collector. Mahian et al. (2013) performed a review of the applications of nanofluids in solar energy. The effects of nanofluids on the performance of solar collectors and solar water heaters from the efficiency, economic and environmental consideration viewpoints and the challenges of using nanofluids in solar energy devices were discussed.

Natarajan and Sathish (2009) studied role of nanofluids in solar water heater. Heat transfer enhancement in solar devices is one of the key issues of energy saving and compact designs. The aim of this paper was to analyze and compare the heat transfer properties of the nanofluids with the conventional fluids. Eismann and Prasser (2013) investigated correction for the absorber edge effect in analytical models of flat plate solar collectors. They derived a new correlation for the fin efficiency. Their correlation was easy to use for engineering purposes. The correlation allowed for more accurate efficiency/cost optimization. One of the major uncertainties of analytical models was eliminated. Wei et al. (2013) studied flat-plate solar heat collector with an integrated heat pipe. An improved structure of flat-plate solar heat collector applied in construction of the solar water heater system was proposed in this paper where the collector used one large integrated wickless heat pipe instead of side-by-side separate heat pipes. High stability and leak avoidance between the water cooling side and the solar heating side were the main advantages in their system.

Nasrin and Alim (2012, 2013) studied free and forced convective heat and mass transfer with entropy generation of nanofluid having single as well as double nanoparticles considering different geometry namely complicated cavity, direct absorption solar collector, prism shaped

solar collector, solar collector having wavy absorber, flat plate solar collector etc. They analyzed nanofluid flow with double nanoparticles using necessary modification of established nanoparticles effective properties. They showed how to enhance thermal performance of different types of solar collectors in their analyses.

In literature review, it is seen that there has been a good number of works in the field of heat transfer system through a flat plate solar collector. But there is some scope to work with temperature, heat transfer and enhancement of collector efficiency using nanofluid. In this paper, the forced convection flow through the riser pipe of a flat plate solar collector is studied numerically. The objective of this paper is to present temperature and velocity profiles as well as heat transfer system for the variation of Prandtl number.

2. PROBLEM FORMULATION

If I be the intensity of solar radiation, incident on the aperture plane of the solar collector having a collector surface area of A , then the amount of solar radiation received by the collector is:

$$Q_i = IA. \quad (1)$$

Basically, it is the product of the rate of transmission of the cover (λ) and the absorption rate of the absorber (κ). Thus,

$$Q_{recv} = I(\lambda\kappa)A. \quad (2)$$

As the collector absorbs heat its temperature is getting higher than that of the surrounding and heat is lost to the atmosphere by convection and radiation. The rate of heat loss (Q_{loss}) depends on the collector overall heat transfer coefficient (U_l), the collector temperature (T_{col}) and ambient temperature (T_{amb}). So,

$$Q_{loss} = U_l A (T_{col} - T_{amb}). \quad (3)$$

Thus, the rate of useful energy extracted by the collector (Q_{usfl}), expressed as a rate of extraction under steady state conditions, proportional to the rate of useful energy absorbed by the collector, less the amount lost by the collector to its surroundings. This is expressed as:

$$Q_{usfl} = Q_{recv} - Q_{loss} = I(\lambda\kappa)A - U_l A (T_{col} - T_{amb}). \quad (4)$$

It is also known that the rate of extraction of heat from the collector may be measured by means of the amount of heat carried away in the fluid passed through it. Thus,

$$Q_{usfl} = mC_p (T_{out} - T_{in}), \quad (5)$$

where m , C_p , T_{in} and T_{out} mass flow rate, specific heat at constant pressure, inlet and outlet fluid temperature respectively.

Equation (4) may be inconvenient because of the difficulty in defining the collector average temperature. It is convenient to define a quantity that relates the actual useful energy gain of a collector to the useful gain if the whole collector surface were at the fluid inlet temperature. This quantity is known as “the collector heat removal factor (F_R)” and is expressed as:

$$F_R = \frac{mC_p(T_{out} - T_{in})}{A[I(\lambda\kappa) - U_l(T_{in} - T_{amb})]} \quad (6)$$

The maximum possible useful energy gain in a solar collector occurs when the whole collector is at the inlet fluid temperature. The actual useful energy gain (Q_{usfl}), is found by multiplying the collector heat removal factor (F_R) by the maximum possible useful energy gain. This allows the rewriting of equation (4) as:

$$Q_{usfl} = F_R A [I(\lambda\kappa) - U_l(T_{in} - T_{amb})] \quad (7)$$

The heat flux per unit area q is now denoted as

$$\frac{Q_{usfl}}{A} = q = I\lambda\kappa - U_l(T_{in} - T_{amb}) \quad (8)$$

Equation (7) is a widely used relationship for measuring collector energy gain and is generally known as the “**Hottel-Whillier-Bliss equation**”.

The instantaneous thermal efficiency of the collector is:

$$\eta = \frac{Q_{usfl}}{AI} = \frac{F_R A [I(\lambda\kappa) - U_l(T_{in} - T_{amb})]}{AI} = F_R(\lambda\kappa) - F_R U_l \frac{(T_{in} - T_{amb})}{I} \quad (9)$$

A schematic diagram of the system and its cross sectional views are shown in Figures 1 (i)-(ii). The numerical computation is carried on taking single riser pipe of FPSC. FPSC with single riser pipe gives the average heat transfer and fluid flow phenomena. Glass cover is at the top of the FPSC. It is made up of borosilicate which has thermal conductivity of 1.14 W/mK and refractive index of 1.47, specific heat of 750 J/kgK and coefficient of sunlight transmission of 95%. The wavelength of visible light is roughly 700 nm. Thickness of glass cover is 0.005m. There is an air gap of 0.005m between glass cover and absorber plate. Air density = 1.269 Kg/m³, specific heat = 287.058 J/kgK and thermal conductivity = 0.0243 W/mK. All these properties of air domain represent air of temperature at 298K. A dark colored copper absorber plate is under the air gap. Length, width and thickness of the absorber plate are 1m, 0.15m and 0.0005m

respectively. Coefficients of heat absorption and emission of copper absorber plate are 95% and 5% respectively.

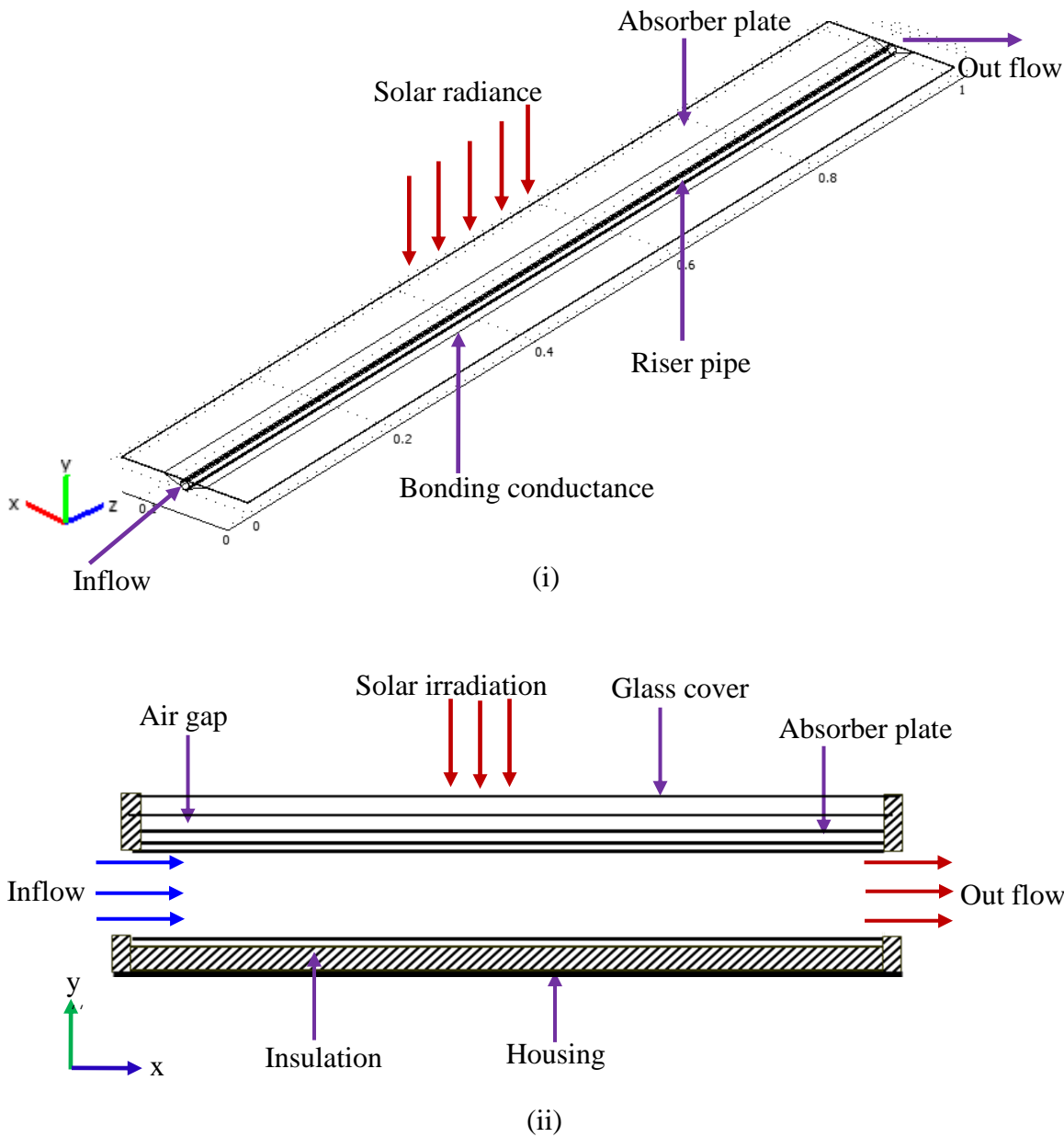


Figure 1. Computational domain of the FPSC (i) 3D and (ii) 2D longitudinal views

The riser pipe has inner diameter 0.01 m and thickness 0.0005m. The riser tube is also made in copper metal. A trapezium shaped bonding conductance of copper metal is attached to the absorber and riser pipe. The fluid through the copper riser pipe is water-based nanofluid containing Al₂O₃ nanoparticles whose thermo-physical properties are shown in Table 1.

The two dimensional governing equations are:

$$\frac{\partial u}{\partial x} + \frac{\partial v}{\partial y} = 0, \quad (10)$$

$$\rho_{nf} \left(u \frac{\partial u}{\partial x} + v \frac{\partial u}{\partial y} \right) = -\frac{\partial p}{\partial x} + \mu_{nf} \left(\frac{\partial^2 u}{\partial x^2} + \frac{\partial^2 u}{\partial y^2} \right), \quad (11)$$

$$\rho_{nf} \left(u \frac{\partial v}{\partial x} + v \frac{\partial v}{\partial y} \right) = -\frac{\partial p}{\partial y} + \mu_{nf} \left(\frac{\partial^2 v}{\partial x^2} + \frac{\partial^2 v}{\partial y^2} \right), \quad (12)$$

$$u \frac{\partial T}{\partial x} + v \frac{\partial T}{\partial y} = \alpha_{nf} \left(\frac{\partial^2 T}{\partial x^2} + \frac{\partial^2 T}{\partial y^2} \right), \quad (13)$$

$$\left(\frac{\partial^2 T_a}{\partial x^2} + \frac{\partial^2 T_a}{\partial y^2} \right) = 0, \quad (14)$$

where

$$\alpha_{nf} = k_{nf} / (\rho C_p)_{nf}$$

is the thermal diffusivity,

$$\rho_{nf} = (1 - \phi) \rho_f + \phi \rho_s$$

is the density,

$$(\rho C_p)_{nf} = (1 - \phi) (\rho C_p)_f + \phi (\rho C_p)_s$$

is the heat capacitance,

$$\mu_{nf} = \frac{\mu_f}{(1 - \phi)^{2.5}}$$

is the viscosity of Brinkman model (1952),

$$k_{nf} = k_f \frac{k_s + 2k_f - 2\phi(k_f - k_s)}{k_s + 2k_f + \phi(k_f - k_s)}$$

is the thermal conductivity of Maxwell Garnett (MG) model (1904),

$$Pr = \frac{\nu_f}{\alpha_f}$$

is the Prandtl number and

$$Re = \frac{u_{in}L}{\nu_f}$$

is the Reynolds number.

The boundary conditions of the riser pipe are:

at all solid boundaries:

$$u = v = 0,$$

at the solid-fluid interface:

$$k_{nf} \left(\frac{\partial T}{\partial y} \right)_{nf} = k_{solid} \left(\frac{\partial T_a}{\partial y} \right)_{solid},$$

at the inlet boundary:

$$T = T_{in}, u = u_{in},$$

at the outlet boundary: convective boundary condition $p = 0$,
 at the top surface of absorber: heat flux

$$-k_a \frac{\partial T_a}{\partial y} = q = I\tau\kappa - U_l(T_{in} - T_{amb}), \text{ and}$$

at outer surface of riser pipe:

$$\frac{\partial T}{\partial y} = 0.$$

Table 1. Thermo physical properties of fluid and nanoparticles at 300K

Physical Properties	Fluid phase (Water)	Al ₂ O ₃
C_p (J/kgK)	4179	765
ρ (kg/m ³)	997.1	3970
k (W/mK)	0.613	40
$\alpha \times 10^7$ (m ² /s)	1.47	131.7

For water based nanofluid flow the expression of local Nusselt number is as follows:

$$\overline{Nu} = \frac{-k_{nf} \left(\frac{\partial T}{\partial y} \right) \left(\frac{L}{k_f} \right)}{\left(\frac{qL}{k_f} \right)} = - \left(\frac{k_{nf}}{k_f} \right) \left(\frac{k_f}{q} \right) \left(\frac{\partial T}{\partial y} \right). \tag{15}$$

The non-dimensional form of local heat transfer rate at the riser pipe solid surface is

$$\overline{Nu} = -\frac{k_{nf}}{k_f} \frac{\partial \theta}{\partial Y}.$$

The above equations are non-dimensionalized by using the following dimensionless, quantities

$$X = \frac{x}{L}, Y = \frac{y}{L}, \theta = \frac{(T - T_{in})k_f}{qL}.$$

By integrating the local Nusselt number over the riser pipe, the average heat transfer rate of the collector can be written as

$$Nu = \frac{1}{L} \int_0^L \overline{Nu} dX.$$

The mean bulk temperature and average sub domain velocity of the fluid inside the collector may be written as

$$T_{av} = \frac{\iint_A T d\bar{A}}{\iint_A d\bar{A}} = \frac{\iint_A T d\bar{A}}{HL} \quad \text{and} \quad V_{av} = \frac{\iint_A V d\bar{A}}{\iint_A d\bar{A}} = \frac{\iint_A V d\bar{A}}{HL}, \quad (16)$$

where \bar{A} , L , H and V are the area, length and height of the absorber tube, magnitude of subdomain velocity, respectively.

The overall heat transfer loss from the collector is the summation of three separate components, the top loss coefficient, the bottom loss coefficient and the edge loss coefficient. The empirical relations for these coefficients are mentioned by Duffie and Beckman (1991) and Al-Ajlan et al. (2003) as follows:

$$U_l = U_t + U_b + U_e, \quad (17)$$

where U_t is the heat loss coefficient from the top, U_b is the heat loss coefficient from the bottom, and U_e is the heat loss coefficient from the edges of collector. These can be calculated from the following relations:

$$U_t = \left\{ \frac{N}{\frac{C}{T_a} \left[\frac{T_a - T_{amb}}{N + f} \right]^c} + \frac{1}{h_{amb}} \right\}^{-1} + \frac{\sigma(T_a + T_{amb})(T_a^2 + T_{amb}^2)}{\frac{1}{(\varepsilon_a + 0.00591Nh_{amb})} + \frac{2N + f - 1 + 0.13\varepsilon_a - N}{\varepsilon_c}},$$

$$U_b = \frac{k_b}{x_b}, \quad U_e = \frac{U_e A_e}{A} = \frac{k_e}{x_e} \left[\frac{2(L+W)H}{LW} \right],$$

$$C = 520 * (1 - 0.000051\beta^2), \text{ and}$$

$$f = (1 + 0.089h_a - 0.1166h_{amb}\varepsilon_a) * (1 + 0.07866N).$$

3. NUMERICAL IMPLEMENTATION

The Galerkin finite element method Taylor and Hood (1973) and Dechaumphai (1999) is used to solve the non-dimensional governing equations along with boundary conditions. The equation of continuity has been used as a constraint due to mass conservation and this restriction may be used to find the pressure distribution. The finite element method of Reddy (1994) is used to solve the equations (10) - (14), where the pressure P is eliminated by a constraint. The continuity equation is automatically fulfilled for large values of this constraint. Then the velocity components (u, v) and temperature (T) are expanded using a basis set. The Galerkin finite element technique yields the subsequent nonlinear residual equations. Three points Gaussian quadrature is used to evaluate the integrals in these equations. The non-linear residual equations are solved using Newton–Raphson method to determine the coefficients of the expansions.

3.1. Mesh Generation

In the finite element method, the mesh generation is the technique to subdivide a domain into a set of sub-domains, called finite elements, control volume, etc. The discrete locations are defined by the numerical grid, at which the variables are to be calculated. It is basically a discrete representation of the geometric domain on which the problem is to be solved. The computational domains with irregular geometries by a collection of finite elements make the method a valuable practical tool for the solution of boundary value problems arising in various fields of engineering. Figure 2 displays the finite element mesh of the present physical domain.

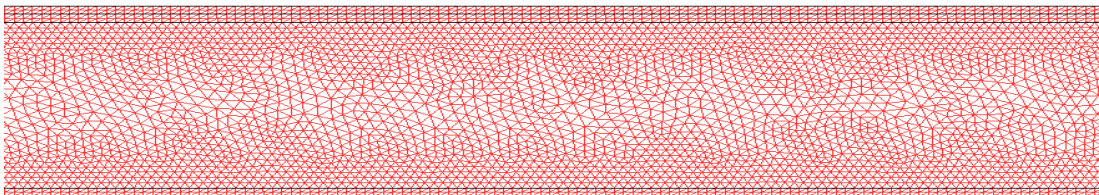


Figure 2. Mesh generation of the computational domain

3.2. Grid Independent Test

An extensive mesh testing procedure is conducted to guarantee a grid-independent solution for $Re = 480$ and $Pr = 5.8$ in a solar collector. In the present work, we examine five different non-uniform grid systems with the following number of elements within the resolution field: 42,010, 99,832, 1,40,472, 1,68,040 and 1,92,548. The numerical scheme is carried out for highly precise key in the average Nusselt number for water-alumina nanofluid ($\phi = 2\%$) as well as base fluid ($\phi = 0\%$) for the aforesaid elements to develop an understanding of the grid fineness as shown in Table 2. The scale of the average Nusselt numbers for nanofluid and clear water for 1,68,040 elements shows a little difference with the results obtained for the other elements. Hence, considering the non-uniform grid system of 1,68,040 elements is preferred for the computation.

Table 2. Grid test at $Pr = 5.8$, $\phi = 2\%$, $I = 215\text{W/m}^2$ and $Re = 480$

Elements	42,010	99,832	1,40,472	1,68,040	1,92,548
Nu (Nanofluid)	1.87872	1.99127	2.10934	2.14351	2.14378
Nu (Base fluid)	1.59326	1.69225	1.81524	1.84333	1.84341
Time (s)	127.52	308.75	581.11	897.23	1295.31

4. RESULTS AND DISCUSSION

Finite element simulation is applied to perform the analysis of laminar forced convection temperature and fluid flow through a riser pipe of a flat plate solar collector filled with water/alumina nanofluid. Effect of the Prandtl number (Pr) on heat transfer and collector efficiency has been studied. The range of Pr for this investigation vary from 4.6 to 6.6 where solar irradiation (I), Reynolds number (Re), and solid volume fraction nanofluid (ϕ) remain fixed at 215 W/m^2 , 480 and 2% respectively. The mass flow rate per unit area (m) is 0.0248 Kg/s, overall heat transfer coefficient (U_l) is $8\text{ W/m}^2\text{K}$, aperture area of the collector (A) is 1.8 m^2 , number of glass (N) is 1, the tilt angle of collector is 0° and nanoparticle size is 10 nm.

Effect of Pr is shown in the Figures 3 (i)-(iii). The streamlines in the Figure 3(i) occupying the whole riser pipe is found at the Prandtl number ($Pr = 5.8$). Color of streamlines at the solid surfaces of riser pipe is deep blue and at the middle is red. This is due to the fact that no-slip condition is maintained at the solid surfaces of riser pipe. Thus maximum velocity is obtained at the middle of the pipe. Also the boundary plot represents that fluid passes through the pipe and takes heat from top surface of riser pipe. That's why boundary temperature becomes low near the inlet and gradually becomes high near the exit boundary. The temperature of top surface of riser pipe is higher than the bottom surface. Arrow plot indicates direction of fluid flow. From Figure

3(iii) it is observed that nanofluid flow enters at the left inlet opening and exits from the right outlet opening.

The effect of Prandtl number (Pr) on average Nusselt number (Nu) at the top of riser pipe, average temperature (T_{av}), magnitude of average velocity (V_{av}), mid-height temperature (T) of water-copper nanofluid, mean outlet temperature (T_{out}) and percentage of collector efficiency with $Re = 480$, $I = 215\text{W/m}^2$, $\phi = 2\%$ are shown in Figures 4(i)-(vi). The values of Pr are chosen as 4.6, 5.2, 5.8 and 6.6.

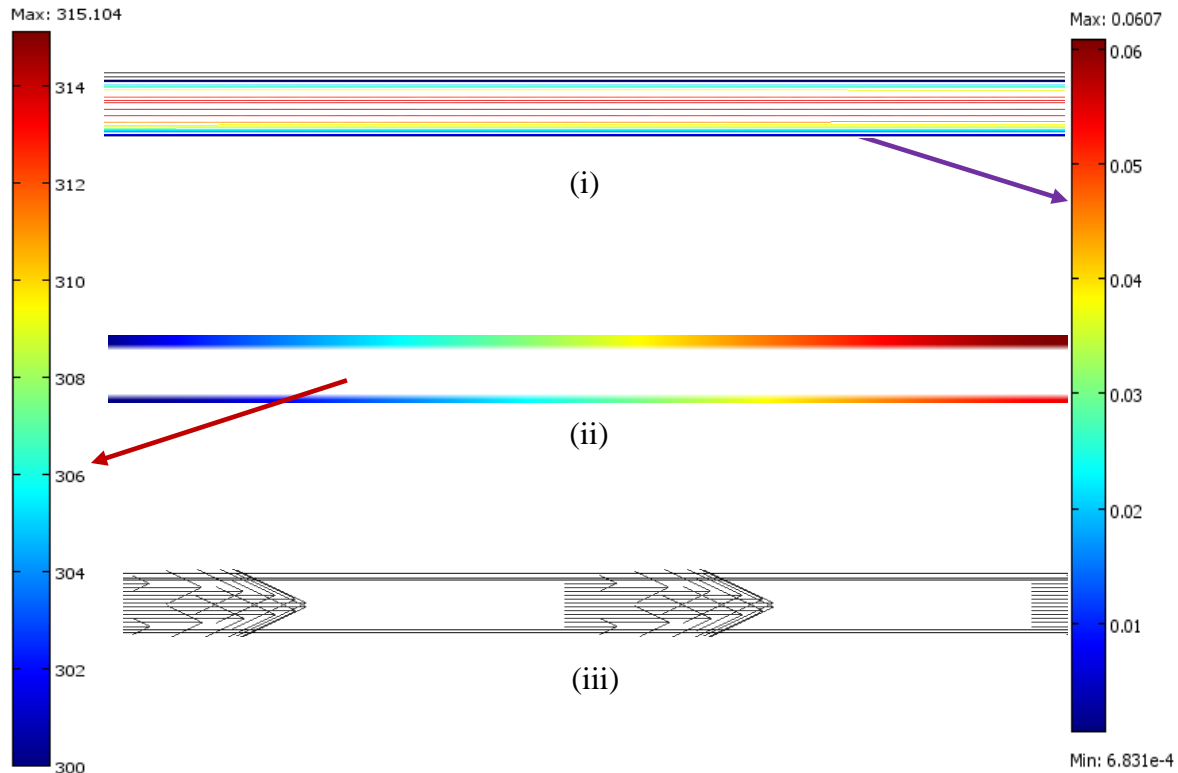


Figure 3: Effect of Pr at 5.8 on (i) streamlines, (ii) boundary plot and (iii) arrow plot

All these values of Prandtl number represent water at different temperatures. From the Figure 4(i) it is clearly observed that as Pr increases, heat transfer rate enhances for both fluids. Nu increases by 16% and 12% with the variation of Pr from 4.6 to 6.6 for water-copper nanofluid and clear water respectively.

As Pr increases average bulk temperature (T_{av}) of the fluids decreases gradually for both fluids. It is well known that increasing Prandtl number devalues fluid temperature. Nanofluid has higher temperature than base fluid.

Mean velocity (V_{av}) devalues for higher Prandtl number because fluid with higher viscosity can't move freely like lower viscous fluid. Water- Al_2O_3 nanofluid has lower mean velocity than clear water.

Temperature (T) of water-Cu nanofluid at the middle of riser pipe is seen in Figure 4(iv). Nanofluid temperature increases when it passes through the riser pipe. But temperature of nanofluid diminishes with growing Pr .

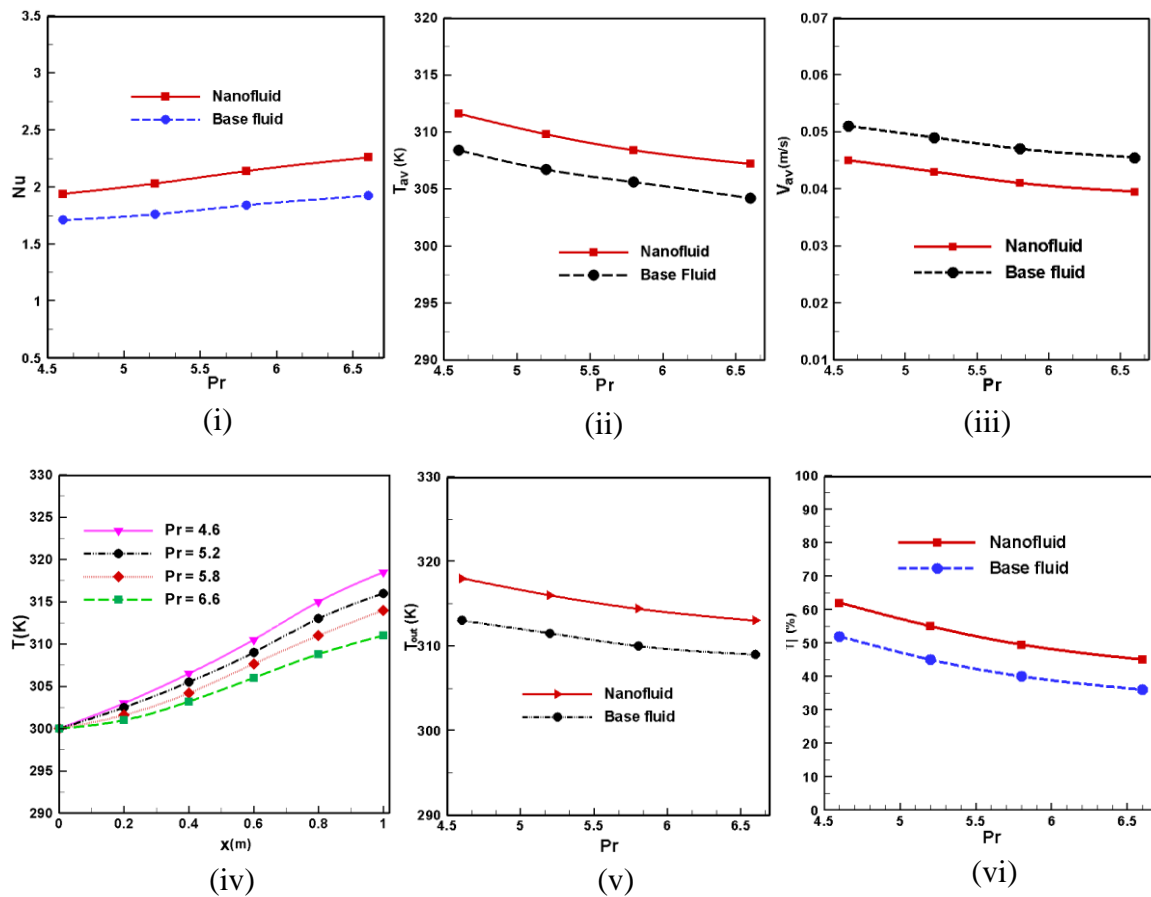


Figure 4. Effect of Pr on (i) mean Nusselt number, (ii) mean bulk temperature, (iii) mean velocity, (iv) mid-height temperature, (v) mean output temperature and (vi) collector efficiency

Figure 4(v) shows that mean outlet temperature (T_{out}) decreases with increasing Prandtl number. This describes in this way that increasing Prandtl number decreases fluid temperature. As a result lower tempered fluid can't become so hot at outlet exit like higher tempered fluid. Average outlet temperature becomes 318K, 316K, 314K, 313K for nanofluid and 313K, 312K, 310K, 309K for water respectively with the variation of $Pr = 4.6, 5.2, 5.8$ and 6.6 .

Using higher values of Prandtl number the collector efficiency decreases. In this scheme water/aluminium oxide nanofluid ($\phi = 2\%$) performs better than clear water ($\phi = 0\%$). Thermal

efficiency devalues from 66%-45% for nanofluid and 52%-36% for water due to the variation of Prandtl number Pr from 4.6 to 6.6.

5. CONCLUSION

The results of the numerical analysis lead to the following conclusions:

The structure of the fluid streamline, boundary plot and arrow plot through the solar collector is found to significantly depend upon the Prandtl number. The Al_2O_3 nanoparticle with the highest Pr is established to be most effective in enhancing performance of heat transfer rate than base fluid. Collector efficiency is obtained lower for growing Pr . Mean bulk temperature diminishes for both fluids with rising Pr . Mean velocity is obtained higher for base fluid with falling Pr .

ACKNOWLEDGEMENT

The present numerical work is done in the Department of Mathematics, Bangladesh University of Engineering & Technology, Dhaka-1000, Bangladesh. Research Support & Publication Division, University Grants Commission, Agargaon, Bangladesh helps financially for this work.

REFERENCES

- Brinkman, H.C. (1952). The viscosity of concentrated suspensions and solution”, *Journal of Chemical Physics*, Vol. 20, pp. 571–581.
- Chabane, F., Moumami, N., Benramache, S., Bensahal, D., Belahssen, O., Lemmadi, F.Z., (2013). Thermal performance optimization of a flat plate solar air heater, *Int. J. of Energy & Tech.*, Vol. 5, No. 8, pp. 1–6.
- Dechaumphai, P. (1999). *Finite Element Method in Engineering*, 2nd ed., Chulalongkorn University Press, Bangkok.
- Eismann, R., Prasser, H.-M. (2013). Correction for the absorber edge effect in analytical models of flat plate solar collectors, *Solar Energy*, Vol. 95, pp. 181–191.
- Mahian, O., Kianifar, A., Kalogirou, S.A., Pop, I., Wongwises, S. (2013). A review of the applications of nanofluids in solar energy, *Int. J. of Heat and Mass Trans.* Vol. 57, pp. 582–594.
- Maxwell-Garnett, J.C., (1904). Colours in metal glasses and in metallic films. *Philos. Trans. Roy. Soc. A*, Vol. 203, pp. 385–420.
- Nasrin, R. and Alim, M.A. (2012). Effect of radiation on convective flow in a tilted solar collector filled with water-alumina nanofluid, *Int. J. of Engg., Sci. & Tech.*, Vol. 4, No. 4, pp. 1-12.
- Nasrin, R. and Alim, M.A. (2012). Prandtl number effect on free convective flow in a solar collector utilizing nanofluid, *Engg. e Transac.*, Vol. 7, No. 2, pp. 62-72.
- Nasrin, R. and Alim, M.A. (2013). Free convective flow of nanofluid having two nanoparticles inside a complicated cavity, *Int. J. of Heat and Mass Trans.*, Vol. 63, pp. 191-198.
- Nasrin, R. and Alim, M.A. (2013). Performance of nanofluids on heat transfer in a wavy solar collector, *Int. J. of Engg., Sci. & Tech.*, Vol. 5, No. 3, pp. 58-77.

- Nasrin, R., Parvin, S. and Alim, M.A. (2013). Buoyant flow of nanofluid for heat-mass transfer through a thin layer, *Mech. Engg. Res. J.*, Vol. 9, pp. 7-12.
- Natarajan, E. & Sathish, R. (2009). Role of nanofluids in solar water heater, *Int. J. Adv. Manuf. Techn.*, Vol. 45, 5 pages. DOI 10.1007/s00170-008-1876-8.
- Reddy, J.N. and Gartling, D.K. (1994). *The Finite Element Method in Heat Transfer and Fluid Dynamics*, CRC Press, Inc., Boca Raton, Florida.
- Sandhu, G. (2013). Experimental study of temperature field in flat-plate collector and heat transfer enhancement with the use of insert devices, M. of Engg. Sci. theseis, The School of Graduate and Postdoctoral Studies, The University of Western Ontario London, Ontario, Canada.
- Struckmann, F. (2008). Analysis of a flat-plate solar collector, Project Report, MVK160 Heat and Mass Transport, Lund, Sweden.
- Taylor, C., Hood, P. (1973). A numerical solution of the Navier-Stokes equations using finite element technique, *Computer and Fluids*, Vol. 1, pp. 73–89.
- Wei, L., Yuan, D., Tang, D., Wu, B. (2013). A study on a flat-plate type of solar heat collector with an integrated heat pipe, *Solar Energy*, Vol. 97, pp. 19–25.
- Zambolin, E. (2011). Theoretical and experimental study of solar thermal collector systems and components, Scuola di Dottorato di Ricerca in Ingegneria Industriale, Indirizzo Fisica Tecnica.

NOMENCLATURES

A	aperture area of solar collector (m^2)
A_e	area base on the perimeter of collector (m^2)
\bar{A}	area of 2D cross section of riser pipe (m^2)
C	constant defined in section 2
C_p	specific heat at constant pressure ($Jkg^{-1}K^{-1}$)
f	friction factor
h	convective heat transfer coefficient ($Wm^{-2}K^{-1}$)
h_a	convective heat transfer coefficient between glass and ambient air ($Wm^{-2}K^{-1}$)
H	height of the collector (m)
I	solar irradiation (Wm^{-2})
k	thermal conductivity of fluid ($Wm^{-1}K^{-1}$)
k_b	back insulation conductivity ($Wm^{-1}K^{-1}$)
k_e	edge insulation conductivity ($Wm^{-1}K^{-1}$)
L	length of the solar collector (m)
N	number of glass
Nu	average Nusselt number
p	pressure ($kgms^{-2}$)
Pr	Prandtl number
q	heat flux (Wm^{-2})
Re	Reynolds number
T	fluid temperature (K)
u, v, w	velocity components along x, y, z direction (ms^{-1})

U_l	overall heat transfer coefficient ($Wm^{-2}K^{-1}$)
V	magnitude of velocity (ms^{-1})
\bar{V}	volume of riser pipe (m^3)
x_b	back insulation thickness (m)
x_e	edge insulation thickness (m)
x, y	Cartesian coordinates (m)
X, Y	dimensionless Cartesian coordinates
W	width of collector (m)

Greek symbols

α	thermal diffusivity (m^2s^{-1})
β	tilt angle ($^\circ$)
λ	transmitivity
ε	emissivity
η	thermal efficiency
ϕ	nanoparticles volume fraction
θ	dimensionless fluid temperature
μ	dynamic viscosity of the fluid (m^2s^{-1})
ν	kinematic viscosity of the fluid (m^2s^{-1})
ρ	density of the fluid (kgm^{-3})
κ	absorption coefficient

Subscripts

a	absorber
amb	ambient
av	average
b	back
c	cover
col	collector
e	edge
f	fluid
in	input
$loss$	lost
nf	nanofluid
out	output
$recv$	received
s	solid particle
t	top
$usfl$	useful